

[Click here to view linked References](#)

Noname manuscript No. (will be inserted by the editor)
--

A Real-Time Path-Planning Algorithm based on Receding Horizon Techniques

M.Murillo · G.Sánchez · L.Genzelis ·

L.Giovanini

Received: date / Accepted: date

1 **Abstract** In this article we present a real-time path-planning algorithm that can
2 be used to generate optimal and feasible paths for any kind of unmanned vehicle
3 (UV). The proposed algorithm is based on the use of a simplified particle vehicle
4 (PV) model, which includes the basic dynamics and constraints of the UV, and an
5 iterated non-linear model predictive control (NMPC) technique that computes the
6 optimal velocity vector ([magnitude](#) and orientation angles) that allows the PV to
7 move towards desired targets. The computed paths are guaranteed to be feasible for
8 any UV because: i) the PV is configured with similar characteristics (dynamics and
9 physical constraints) as the UV, and ii) the feasibility of the optimization problem
10 is guaranteed by the use of the iterated NMPC algorithm. As demonstration of the

M.Murillo · G.Sánchez · L.Genzelis · L.Giovanini

Instituto de Investigación en Señales, Sistemas e Inteligencia Computacional, sinc(i), UNL,
CONICET, Ciudad Universitaria UNL, 4to piso FICH, (S3000) Santa Fe, Argentina.

Tel: +54(342)4575233/34 ext 118. Fax: +54(342)4575224.

E-mail: mmurillo@sinc.unl.edu.ar · gsanchez@sinc.unl.edu.ar · lgenzelis@sinc.unl.edu.ar · lgiovanini@sinc.unl.edu.ar

11 capabilities of the proposed path-planning algorithm, we explore several simulation
12 examples in different scenarios. We consider the existence of static and dynamic
13 obstacles and a follower condition.

14 **Keywords** [feasible optimal path](#) · [model predictive control](#) · [real-time path-](#)
15 [planning](#) · [replanning](#)

16 1 Introduction

17 One of the areas that has grown surprisingly fast in the last decade is the one
18 involving autonomous Unmanned Vehicles (UVs), both aerial (*Unmanned Aerial*
19 *Vehicles* - UAVs) and terrestrial (*Unmanned Ground Vehicles* - UGVs). Their re-
20 duced size and geometry allow them to carry out dangerous missions at lower
21 costs than their manned counterparts without compromising human lives. They
22 are mostly used in missions such as search and rescue, power line inspections,
23 precision agriculture, imagery and data collection, security applications, mine de-
24 tection and neutralization, operations in hazardous environments, among others
25 [1–6]. In general, most of such missions require that the UVs move in uncertain
26 scenarios avoiding different types of obstacles. To do so, they must have the ability
27 to *autonomously* determine and track a feasible collision-free path.

28 The path-planning problem is one of the most important parts of an au-
29 tonomous vehicle, therefore it has attracted substantial attention [7, 8]. It deals
30 with searching a feasible path between the present location and the desired target
31 while taking into consideration the geometry of the vehicle and its surroundings,
32 its kinematic constraints and other factors that may affect the feasible path. Dif-
33 ferent methodologies are used to find feasible paths (see [9] for an overview). Some

34 recent path-planning algorithms can be found in [10–12]. In [10] *Saska et al.* in-
35 troduce a technique that integrates a spline-planning mechanism with a receding
36 horizon control algorithm. This approach makes it possible to achieve a good per-
37 formance in multi-robot systems. In [11] an offline path-planning algorithm for
38 UAVs in complex terrain is presented. The authors propose an algorithm which
39 can be divided into two steps: firstly a probabilistic method is applied for local ob-
40 stacle avoidance and secondly a heuristic search algorithm is used to plan a global
41 trajectory. In [12] *Zhang et al.* present a guidance principle for the path-following
42 control of underactuated ships. They propose to split the path into regular straight
43 lines and smooth arcs, using a virtual guidance ship to obtain the control input
44 references that the real ship should have in order to follow the computed path. As
45 it can be seen, there are many methods to obtain feasible paths for UVs; however,
46 most of them do not consider the dynamics of the UV that should follow the path.

47 In their recent review article [13], *Yang et al.* have surveyed different path-
48 planning algorithms. The authors discuss the fundamentals of the most successful
49 robot 3D path-planning algorithms that have been developed in recent years. They
50 mainly analyze algorithms that can be implemented in aerial robots, ground robots
51 and underwater robots. They classify the different algorithms into five categories:
52 i) sampling based algorithms, ii) node based algorithms, iii) mathematical model
53 based algorithms (which include optimal control and receding horizon strategies),
54 iv) bioinspired algorithms, and v) multifusion based algorithms. From these, only
55 mathematical model based algorithms are able to incorporate in a simple way
56 both the environment (kinematic constraints) and the vehicle dynamics in the
57 path-planning process. Recently, in [14] *Hehn and D'Andrea* introduced a trajec-
58 tory generation algorithm that can compute flight trajectories for quadcopters.

59 The proposed algorithm computes three separate translational trajectories (one
60 for each degree of freedom) and guarantees the individual feasibility of these tra-
61 jectories by deriving decoupled constraints through approximations. The authors
62 do consider the quadcopter dynamics when they compute the flight trajectories
63 but their proposed technique is not a general one (it can not be used with ground
64 vehicles, for example). Even though the feasibility is guaranteed for each separate
65 trajectory, the resulting vehicle trajectory might not be necessarily feasible (e.g.,
66 when perturbations are present). In [15] the authors present three conventional
67 holonomic trajectory generation algorithms (flatness, polynomial and symmetric)
68 for ground vehicles subject to constraints on their steering angle. In order to sat-
69 isfy this constraint, they propose to lengthen the distance from the initial position
70 to the final position until the constraint is satisfied. This process might be tedious
71 and it may not be applicable in dynamic environments. Besides, it can only be
72 used with ground vehicles and it can only handle steering constraints violations.

73 Motivated by the advent of new autonomous vehicles that encompass a broad
74 range of mission capabilities, a suitable path-planning algorithm should be prac-
75 ticable and tailored to various UVs when executed in dynamical environments.
76 Therefore, a challenging idea for path-planning is to develop an algorithm capable
77 of handling dynamical environments and UVs that have different characteristics
78 with regard to kinematic properties and maneuverability. For example, an au-
79 tonomous rotary-wing vehicle is able to stop and make quick turns on a spot. On
80 the contrary, an autonomous fixed-wing aircraft has to maintain a minimal flight
81 velocity and can not turn at a large angle instantaneously. If a path obtained
82 from a planning algorithm demands many agile or abrupt maneuvers, it would be
83 difficult or even completely impossible to track. Consequently, it is inadequate in

84 practice for a planning algorithm to only aim at an invariable model of steady
 85 maneuver.

86 In this article a unified framework to design an online path-planning algorithm
 is presented. The proposed strategy can be summarized in Fig. 1. Using a simplified

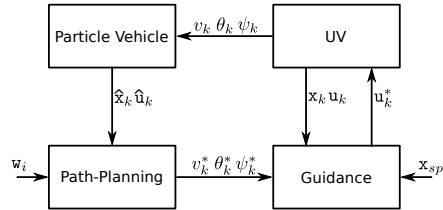


Fig. 1 Scheme of the path-planning & guidance system

87

88 particle vehicle (PV) model, which is configured to have similar characteristics
 89 (states and inputs constraints) to the UV, the path-planning module computes
 90 the velocity vector \mathbf{v}_k^* (magnitude v_k^* and angles θ_k^* and ψ_k^*) in order to find the
 91 shortest feasible path towards the nearest waypoint \mathbf{w}_i . The vector \mathbf{v}_k^* is in fact
 92 the velocity vector that the UV should have in order to achieve \mathbf{w}_i . Thus, using
 93 this velocity vector and other possible setpoints \mathbf{x}_{sp} , the guidance module is able
 94 to compute the inputs (actuator positions and motors speeds) that the UV should
 95 have so as to move towards \mathbf{w}_i . In this article, we mainly focus on the design of
 96 the path-planning module. We propose to design this module using the iterated
 97 robust NMPC technique presented in [16] as it uses a successive linearization
 98 method which allows us to use analytic tools to evaluate stability, robustness and
 99 convergence issues. Besides, it allows us to use quadratic program (QP) solvers
 100 and to easily take into account dynamic and physical constraints of the UV at the
 101 path-planning stage in order to obtain feasible paths.

102 The main contribution of this paper are: i) the proposal of a general algorithm
 103 for path-planning that can be used with any kind of UV, ii) the inclusion of
 104 the dynamics and constraints of the UV in the path-planning problem, iii) the
 105 guarantee of feasibility of the computed optimal path, iv) the inclusion of static
 106 and dynamic obstacles into the path planning problem, and v) the decentralization
 107 of the path-planning problem for multiple vehicles.

108 The organization of this article is as follows: in section 2 the 2D and 3D PV
 109 models are presented. In section 3, the path-planning problem is introduced. In
 110 section 4 three simulation examples are outlined. Finally, in section 5 conclusions
 111 are presented.

112 **2 Non-linear Particle Vehicle Model**

113 In this work we propose to use a PV model to obtain feasible and optimal paths
 114 for UVs. This section is devoted to obtain such a model for both the 2D and 3D
 115 cases. First, we provide a more general approach about systems representation and
 116 then we particularize it for the case of 2D and 3D PV models.

117 The general representation of the dynamics of an arbitrary non-linear system
 118 is given by

$$119 \quad \dot{\mathbf{x}}(t) = f(\mathbf{x}(t), \mathbf{u}(t), \mathbf{d}(t)), \quad (1)$$

120 where $\mathbf{x}(t) \in \mathcal{X} \subseteq \mathbb{R}^n$, $\mathbf{u}(t) \in \mathcal{U} \subseteq \mathbb{R}^m$ and $\mathbf{d}(t) \in \mathcal{D} \subseteq \mathbb{R}^v$ are the model state,
 121 input and disturbance vectors, respectively; \mathcal{X} , \mathcal{U} and \mathcal{D} are the state, input and

122 disturbance constraint sets; $f(\cdot)$ is a continuous and twice differentiable vector
 123 function that depends on the system being modeled¹.

124 To obtain the PV models, we use the 2D and 3D schemes shown in Fig. 2.
 Using these schemes, we propose to use the following state vector to model the 2D

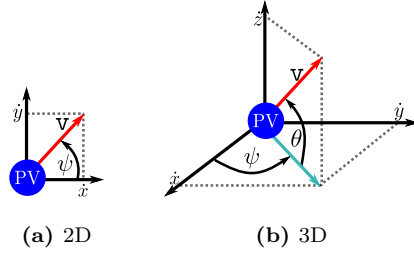


Fig. 2 Schemes of the proposed PV models

125

126 PV

127

$$\mathbf{x} = [x, y, v]^T, \quad (2)$$

128 where x and y denote the PV position coordinates and v is the modulus of the PV
 129 velocity vector. We define the control input vector as

130

$$\mathbf{u} = [\psi, \mathcal{T}]^T, \quad (3)$$

131 where ψ and \mathcal{T} denote the yaw angle and the thrust force, respectively. Conse-
 132 quently, the 2D dynamics of the proposed PV model can be obtained as

133

$$\dot{\mathbf{x}} = f(\mathbf{x}, \mathbf{u}, \mathbf{d}) = \begin{bmatrix} v \cos \psi + d_x \\ v \sin \psi + d_y \\ -\tau v + \kappa \mathcal{T} \end{bmatrix}, \quad (4)$$

¹ To simplify the notation, from now on we will omit the time dependence, i.e. $\dot{\mathbf{x}}(t) = \dot{\mathbf{x}}$, $\mathbf{x}(t) = \mathbf{x}$, $\mathbf{u}(t) = \mathbf{u}$ and $\mathbf{d}(t) = \mathbf{d}$

134 where d_x and d_y are the xy components of \mathbf{d} , the damping constant τ determines
 135 the rate of change of the PV velocity and κ is a constant proportional to the thrust
 136 force \mathcal{T} .

137 To model the 3D PV we just have to include the altitude dependence. Using
 138 the scheme presented in Fig. 2b, the state vector is chosen as

$$139 \quad \mathbf{x} = [x, y, z, v]^T, \quad (5)$$

140 where x , y and z denote the PV position coordinates and v is the modulus of the
 141 PV velocity vector. The control input vector is then defined as

$$142 \quad \mathbf{u} = [\theta, \psi, \mathcal{T}]^T, \quad (6)$$

143 where θ , ψ and \mathcal{T} denote, respectively, the pitch angle, the yaw angle and the
 144 thrust force. Then, the 3D dynamics of the PV model can be described by the
 145 following first order differential equation system:

$$146 \quad \dot{\mathbf{x}} = f(\mathbf{x}, \mathbf{u}, \mathbf{d}) = \begin{bmatrix} v \cos \theta \cos \psi + d_x \\ v \cos \theta \sin \psi + d_y \\ v \sin \theta + d_z \\ -\tau v + \kappa \mathcal{T} \end{bmatrix}, \quad (7)$$

147 where d_x , d_y and d_z are the xyz components of \mathbf{d} . As it can be seen, if the pitch
 148 angle θ is zero, then (7) is reduced to (4).

149 One important thing we would like to mention about the proposed PV models is
 150 that in the last equation of (4) and (7) the basic dynamics of the UV is included.
 151 This is very advantageous as physical systems do not have the ability to make
 152 instant changes in their dynamics. So, by including this last equation in the PV
 153 models we ensure that if this model is used in the path-planning module, then

154 the path will be computed reflecting the UV basic dynamics, and consequently
 155 guaranteeing the feasibility of the path. Generally, the UV dynamics is not taken
 156 into account in path-planning algorithms because they use impulsional models
 157 [12, 17], which can lead to unfeasible paths for a UV.

158 3 The Path-Planning Problem

159 Given a target position or *waypoint* \mathbf{w}_i the path-planning problem consists in
 160 finding a path that connects the initial state vector $\mathbf{x}(t_0)$ and each consecutive
 161 waypoint \mathbf{w}_i^2 , where the subscript $i = 1, 2, \dots, M$ indicates the waypoint number.
 162 In this article we propose to find the path that is not only the shortest one but
 163 also a feasible one, i.e. the shortest path that also takes into account the dynam-
 164 ics and physical constraints of the UV that should follow the path. To find the
 165 shortest path we only have to measure the distance between the current position
 166 of the PV and the desired waypoint, and then minimize it. But as we also want
 167 the path to be feasible, we have to include the dynamics and constraints in the
 168 minimization problem. This may be done, for example, using a receding horizon
 169 technique, since the distance can be embedded in the cost function and the dy-
 170 namics and constraints in the constrained minimization. Here, we propose to use
 171 the NMPC technique presented in [16] to control the velocity vector (modulus and
 172 direction) of the PV model. By controlling this vector the position of the PV is
 173 actually determined, thus defining the desired path towards the waypoint. The
 174 main advantage of using this technique (unlike the one used in [12], for example)

² For the 2D case \mathbf{w}_i is defined as $\mathbf{w}_i = [w_{i_x}, w_{i_y}, w_{i_v}]^T$ and for the 3D case $\mathbf{w}_i = [w_{i_x}, w_{i_y}, w_{i_z}, w_{i_v}]^T$. w_{i_x} , w_{i_y} and w_{i_z} denote the xyz coordinates of waypoint \mathbf{w}_i and w_{i_v} defines the speed that the PV should have when \mathbf{w}_i is reached.

175 is that, as the dynamics and constraints of the UV that should follow the path
 176 can be taken into account in the minimization problem, then the resulting path is
 177 guaranteed to be feasible.

In Fig. 3 a scheme of the proposed methodology is shown. Under the assump-

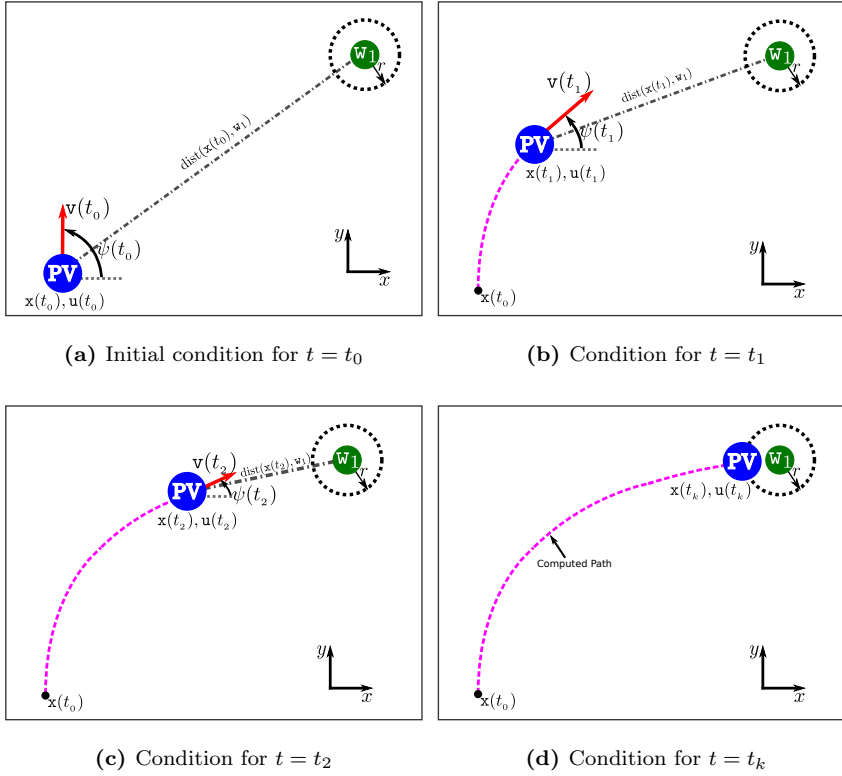


Fig. 3 Computing a path between $\mathbf{x}(t_0)$ and \mathbf{w}_1

178

179 tion that the control inputs of the PV have a limited rate of change, this figure
 180 shows how the path towards a single waypoint \mathbf{w}_1 is obtained. As can be seen in
 181 Figs. 3b and 3c, the PV starts moving towards \mathbf{w}_1 . To do this, we propose to use
 182 the algorithm [16] to minimize the euclidean distance ($\text{dist}(\mathbf{x}(t_j), \mathbf{w}_i)$) between the

183 current position of the PV and the desired waypoint. As a result, the optimal yaw
 184 angle and thrust force are computed and the velocity vector modifies its direction
 185 and modulus in order to reach the desired target in a feasible way. The path we
 186 were looking for turns out to be the path that the PV has described in order to
 187 go from the starting configuration to the desired one (see Fig. 3d).

188 Also, it could happen that a path that connects the initial position and several
 189 waypoints is required. This situation is illustrated in Fig. 4 for the case of two
 190 waypoints³. As shown in Fig. 4a, the PV is configured with an initial condition
 191 $\mathbf{x}(t_0)$, $\mathbf{u}(t_0)$ and the path should pass first through the waypoint \mathbf{w}_1 and then
 192 through the waypoint \mathbf{w}_2 . To obtain this path, two sub-paths are considered: one
 193 joining the initial configuration with \mathbf{w}_1 and the other joining \mathbf{w}_1 with \mathbf{w}_2 . The
 194 first sub-path is obtained in a similar way as we have done in Fig. 3. Once \mathbf{w}_1
 195 has been reached, the second sub-path can be computed. To do this, the desired
 196 target is changed from \mathbf{w}_1 to \mathbf{w}_2 and the minimization of the distance between the
 197 current position of the PV and \mathbf{w}_2 is performed. As a result, the PV starts moving
 198 again and its velocity vector is recalculated in order to move the PV towards \mathbf{w}_2
 199 (see Figs. 4b and 4c). The full computed path can be seen in Fig. 4d. As it is
 200 shown, it has been obtained by joining both sub-paths together.

201 As was mentioned before, we propose to modify the direction and modulus of
 202 the velocity vector of the PV using the control technique described in [16]. To use
 203 this control technique, first we need to transform the non-linear model (1) into an
 204 equivalent discrete linear time-varying (LTV) one of the form

$$205 \quad \tilde{\mathbf{x}}_{k+1|k} = \mathbf{A}_{k|k} \tilde{\mathbf{x}}_{k|k} + \mathbf{B}_{u_{k|k}} \tilde{\mathbf{u}}_{k|k} + \mathbf{B}_{d_{k|k}} \tilde{\mathbf{d}}_{k|k}, \quad (8)$$

³ Note that if there are more than two waypoints, the procedure to compute the path is similar as the one presented here.

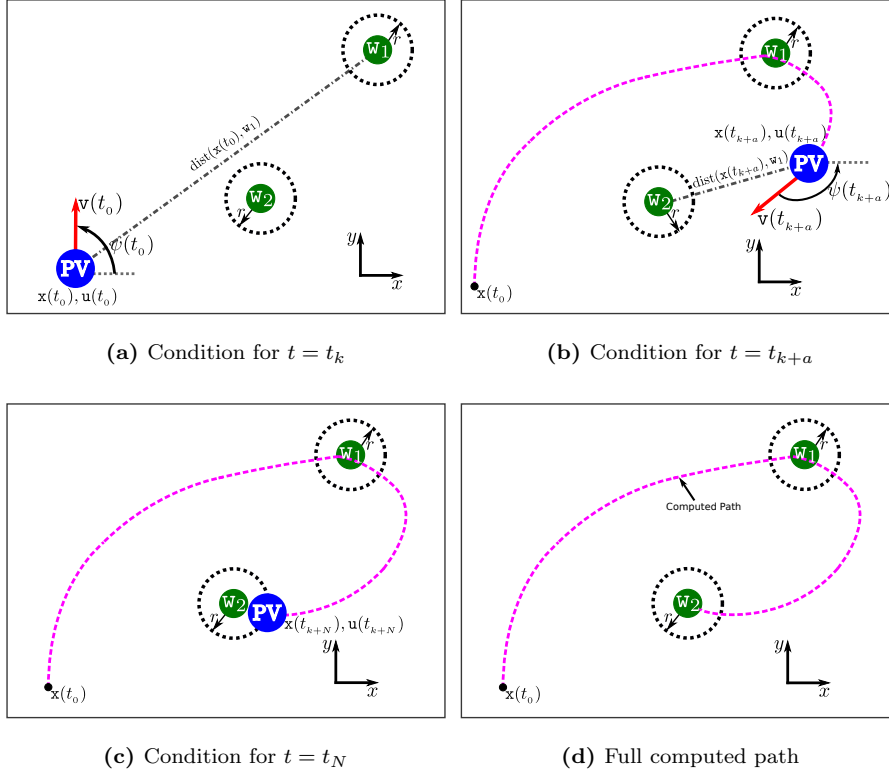


Fig. 4 Computing a path between $\mathbf{x}(t_0)$ and \mathbf{w}_2 passing through \mathbf{w}_1

206 where

$$207 \quad \tilde{\mathbf{x}}_{k|k} = \mathbf{x}_{k|k} - \mathbf{x}_{k|k}^r, \quad \tilde{\mathbf{u}}_{k|k} = \mathbf{u}_{k|k} - \mathbf{u}_{k|k}^r \quad \text{and} \quad \tilde{\mathbf{d}}_{k|k} = \mathbf{d}_{k|k} - \mathbf{d}_{k|k}^r. \quad (9)$$

208 $\mathbf{x}_{k|k}^r$, $\mathbf{u}_{k|k}^r$ and $\mathbf{d}_{k|k}^r$ ⁴ define the linearization state, input and disturbance **trajecto-**
 209 **ries**, and $\mathbf{A}_{k|k}$, $\mathbf{B}_{u_{k|k}}$ and $\mathbf{B}_{d_{k|k}}$ are **the discrete matrices of the linearized version**
 210 **of (1)**. Receding horizon techniques use a cost function of the form

$$211 \quad \mathcal{J}(k) = \sum_{j=0}^{N-1} \mathcal{L}_j(\mathbf{x}_{k+j|k}, \mathbf{u}_{k+j|k}) + \mathcal{L}_N(\mathbf{x}_{k+N|k}), \quad (10)$$

⁴ $\mathbf{d}_{k+j|k}^r$, $j = 0, \dots, N-1$ is a given or estimated perturbation

212 where $\mathcal{L}_j(\cdot, \cdot)$ is the stage cost and $\mathcal{L}_N(\cdot, \cdot)$ stands for the terminal cost. Gener-
 213 ally, in receding horizon algorithms both the stage cost and the terminal cost are
 214 adopted as follows:

$$215 \quad \mathcal{L}_j(\mathbf{x}_{k+j|k}, \mathbf{u}_{k+j|k}) = \|\mathbf{x}_{k+j|k} - \mathbf{w}_i\|_{\mathbf{Q}_{k|k}}^l + \|\Delta \mathbf{u}_{k+j|k}\|_{\mathbf{R}_{k|k}}^p \quad (11)$$

216 and

$$217 \quad \mathcal{L}_N(\mathbf{x}_{k+N|k}) = \|\mathbf{x}_{k+N|k} - \mathbf{w}_i\|_{\mathbf{P}_{k|k}}^l, \quad (12)$$

218 where $\mathbf{Q}_{k|k}$, $\mathbf{R}_{k|k}$, $\mathbf{P}_{k|k}$ are positive definite matrices; $\mathbf{P}_{k|k}$ is the terminal weight
 219 matrix that is chosen so as to satisfy the Lyapunov equation. Superscripts l and p
 220 are even positive numbers and in general are adopted as $l = p = 2$. $\|\cdot\|_{\alpha}^{\beta}$ stands
 221 for the α -weighted β -norm and $\Delta \mathbf{u}_{k+j|k} = \mathbf{u}_{k+j|k} - \mathbf{u}_{k+j-1|k}$. Then, in terms
 222 of the LTV system (8) and according to [16], we propose to solve the following
 223 optimization problem:

$$224 \quad \begin{aligned} & \min_{\tilde{\mathbf{U}}_k \in \mathcal{U}} \mathcal{J}(k) \\ \text{st.} & \begin{cases} \tilde{\mathbf{x}}_{k+j|k} = \mathbf{A}_{k|k} \tilde{\mathbf{x}}_{k|k} + \mathbf{B}_{k|k} \tilde{\mathbf{u}}_{k|k}, \\ \tilde{\mathbf{x}}_{k|k} = \mathbf{x}_{k|k} - \mathbf{x}_{k|k}^r, \\ \tilde{\mathbf{u}}_{k|k} = \mathbf{u}_{k|k} - \mathbf{u}_{k|k}^r, \\ \mathcal{J}(k) \leq \mathcal{J}_0(k). \end{cases} \end{aligned} \quad (13)$$

225 where

$$226 \quad \tilde{\mathbf{U}}_k^5 = [\tilde{\mathbf{u}}_{k|k}, \tilde{\mathbf{u}}_{k+1|k}, \dots, \tilde{\mathbf{u}}_{k+N-1|k}]^T \quad (14)$$

227 is the control input sequence and $\mathcal{J}_0(k)$ denotes the cost function evaluated for
 228 the initial solution $\mathbf{U}_k^0 = [\mathbf{u}_{k|k-1}, \mathbf{u}_{k+1|k-1}, \dots, \mathbf{u}_{k+N-2|k-1}, 0]^T$ at iteration k .

⁵ Hereinafter we use bold capital fonts to denote complete sequences computed for $k, k + 1, \dots, k + N - 1$.

229 The last inequality in (13) defines the contractive constraint that guarantees the
 230 convergence of the iterative solution and defines an upper bound for $\mathcal{J}(k)$ (for a
 231 detailed explanation about this contractive constraint, please refer to [16]).

232 In this work, we propose to split the optimization problem (13) into two dif-
 233 ferent ones. When the current position of the PV is far away from the desired
 234 waypoint (that is to say when $\text{dist}^6(\mathbf{x}_{k|k}, \mathbf{w}_i) > r$) we use the standard quadratic
 235 objective function, i.e. we set $l = 2$ and $p = 2$ ⁷. Instead, when the current position
 236 of the PV is sufficiently close to the desired waypoint (say $\text{dist}(\mathbf{x}_{k|k}, \mathbf{w}_i) \leq r$) we
 237 adopt a higher order objective function, i.e we set $l = 4$ and $p = 2$.

238 *Remark 1* Note that with the selected values of l and p both optimization problems
 239 are convex, thus not affecting the optimality, feasibility and stability of the system.

240 The main idea behind changing the order of the optimization problem can be
 241 explained looking at Fig. 5. This figure shows how the one dimensional (1D) cost
 242 function

$$243 \quad c(e) = \left(\frac{e - w_i}{r} \right)^l \quad (15)$$

244 changes its shape as the parameter l is varied. As it can be seen, when we are
 245 sufficiently close to the desired waypoint, as l gets bigger the derivative of the cost

⁶ $\text{dist}(a, b)$ is a function that computes the euclidean distance between a and b . r is the radius of a circumference (2D case) or a sphere (3D case) centred at \mathbf{w}_i that defines the zone in which we consider that we are close enough to the waypoint and proceed to follow the next one.

⁷ Note that with $l = 2$ the position error for both the stage cost and the terminal cost are the square of the distance between the current position and the desired one, which is the quantity we want to minimize. $p = 2$ was selected in order to obtain a quadratic function for input variations. Also, with the proposed superscripts selection, the cost function can be seen as a measure of the energy expended in the path-planning process.

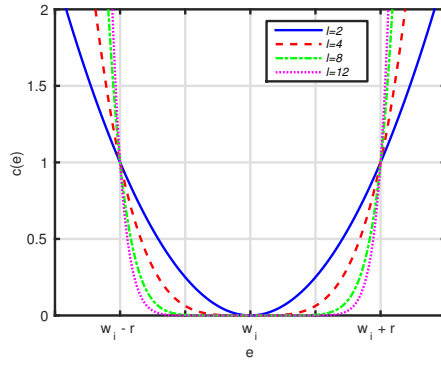


Fig. 5 One dimensional cost function

246 function around $e = w_i \pm r$ is very sharp. This effect can be used to force the PV
 247 to reach the desired waypoint faster than if the conventional quadratic function
 248 ($l = 2$) is used. For the multi-dimensional case, the effect of varying l is similar as
 249 the one described for the 1D case. We have discussed the 1D case because it can
 250 be visualized graphically.

251 The proposed path-planning algorithm can be described as follows: first, the
 252 non-linear system is transformed into a LTV system by means of successive lin-
 253 earizations along pre-defined state-space trajectories. Then, the distance between
 254 the current position of the PV and the desired waypoint is measured. If the PV is
 255 close enough to the target, then the higher order optimization problem is adopted
 256 to force the PV to reach the waypoint faster than if the conventional optimization
 257 problem is used. The proposed constrained minimization problem is solved and
 258 the optimal control input sequence (orientation angles and thrust force) is then
 259 obtained. The minimization process is repeated until the control input sequence
 260 converges. Finally, the computed optimal inputs are applied to the PV and the

261 path-planning process is reinitialized. In Algorithm 1, the proposed path-planning
 262 algorithm is summarized.

263 *Remark 2* Note that the change in the objective function does not affect the con-
 264 vergence and stability because $\mathcal{J}(k) \leq \mathcal{J}_0(k)$ guarantees these properties for time-
 265 variant objective functions [16].

266 *Remark 3* If multiple vehicles are considered in the path-planning procedure, the
 267 proposed algorithm can be used in a decentralized manner because the couplings
 268 between vehicles can be embedded into the objective function and the constraints
 269 of the minimization problem [18].

270 4 Simulation Examples

271 In this section several simulation examples are shown. Using the PV model (4) we
 272 solve the optimization problem (13) to find 2D feasible and optimal paths. The
 273 extension to the 3D case is straightforward, we only need to use the PV model (7)
 274 instead of (4).

275 For all the simulation examples we assumed that there are no disturbances
 276 ($\mathbf{d}_{k|k} = 0$) and that the PV has the initial state vector $\mathbf{x}_0 = [0, 0, 0]^T$ and the
 277 initial input vector is $\mathbf{u}_0 = [\pi/2, 0]^T$. The PV model is discretized using a sampling
 278 rate $T_s = 0.1$ s and the horizon N was set to $N = 8$. The input weight matrix is
 279 chosen as $\mathbf{R}_{k|k} = \text{diag}([0.1, 0.1])$. The PV constraints are configured as follows:
 280 $0 \leq \mathcal{T} \leq 2$ (N), $-0.087 \leq \Delta\psi \leq 0.087$ (rad/s), $-1 \leq \Delta\mathcal{T} \leq 1$ (N/s) and $0 \leq v \leq$
 281 2 (m/s). ψ , x and y are unconstrained. Both constants of the PV model are set as
 282 $\tau = 2$ (1/s) and $\kappa = 2$ (1/kg). As we are interested in having the computed path

Algorithm 1: The Path-planning algorithm

Require: The initial condition $\mathbf{x}_{k|k}$, the iteration index $q = 0$ and the PV models (4) or (7)

- 1: Obtain the LTV system $[\mathbf{A}_{k|k}, \mathbf{B}_{k|k}]$ and the matrices $Q_{k|k}^q$, $R_{k|k}^q$ and $P_{k|k}^q$.
- 2: **if** $\text{dist}(\mathbf{x}_{k|k}, \mathbf{w}_i) > r$ **then**
- 3: $l \leftarrow 2$
- 4: $p \leftarrow 2$
- 5: **else**
- 6: $l \leftarrow 4$
- 7: $p \leftarrow 2$
- 8: **end if**
- 9: Compute the optimal control input sequence $\tilde{\mathbf{U}}_k^{*,q}$ solving (13)
- 10: Update $\mathbf{U}_{k|k}^{*,q} \leftarrow \mathbf{U}_{k|k}^{r,q} + \tilde{\mathbf{U}}_k^{*,q}$
- 11: **if** $\|\mathbf{U}_k^{*,q} - \mathbf{U}_k^{*,q-1}\|_\infty \leq \epsilon$ **then**
- 12: $\mathbf{U}_k^* \leftarrow \mathbf{U}_k^{*,q}$
- 13: $k \leftarrow k + 1$
- 14: $q \leftarrow 0$
- 15: **else**
- 16: $q \leftarrow q + 1$
- 17: Update $\mathbf{U}_k^q = \mathbf{U}_k^{*,q-1}$
- 18: Go back to line 2
- 19: **end if**
- 20: Apply $\mathbf{u}_{k|k} = \mathbf{u}_{k|k}^*$ to the system
- 21: Go back to line 1

283 pass sufficiently close to the waypoints, but not exactly through them, we define
 284 a circular area centered at each waypoint. If the path passes through this area,
 285 then we consider that the corresponding waypoint has been reached. For all the
 286 waypoints we set this area to a disk with a radius of $r = 0.4$ (m).

287 In examples 1 and 2 we assume that the computed path should pass sufficiently
 288 close to the following three waypoints⁸:

$$\begin{aligned}
 \mathbf{w}_1 &= [-10, 0, 1]^T, \\
 \mathbf{w}_2 &= [3, 8, 1]^T, \\
 \mathbf{w}_3 &= [-2, -5, 0]^T.
 \end{aligned}
 \tag{16}$$

290 For these examples, the weight matrices are adopted as follows:

- 291 1. Between the initial position \mathbf{x}_0 and the first waypoint \mathbf{w}_1 , the state weight
 292 matrix is adopted as $\mathbf{Q}_{k|k} = \text{diag}([10, 10, 10])$.
- 293 2. Between the waypoints \mathbf{w}_1 and \mathbf{w}_2 , we adopt $\mathbf{Q}_{k|k} = \text{diag}([10, 10, 100])$.
- 294 3. Between the waypoints \mathbf{w}_2 and \mathbf{w}_3 , the weight matrix is adopted as $\mathbf{Q}_{k|k} =$
 295 $\text{diag}([10, 10, 100])$.

296 In example 3 we assume that the computed path should pass sufficiently close
 297 to the following waypoint:

$$\mathbf{w}_1 = [10, 8, 0]^T.
 \tag{17}$$

299 For this example, the weight matrix is adopted as $\mathbf{Q}_{k|k} = \text{diag}([10, 10, 10])$.

300 At this point it is worth mentioning that with the proposed approach all the
 301 examples could be run in real-time, as the optimization loop was solved in a max-
 302 imum time of approximately 30 (ms) in a desktop PC (i7-2600K CPU@3.40GHz,
 303 32GB RAM). All the examples were programmed using Python and CasADi [19]
 304 and were not optimized in any way. Since CasADi has C++ interfaces, we think
 305 that there is still room for improvement.

⁸ As the simulation examples are performed for the 2D case, the components of the following waypoints denote, respectively, x -coordinate, y -coordinate and speed.

306 4.1 Example 1

307 In this example we use the PV model (4) to compute a feasible and optimal path
 308 that passes sufficiently close to the waypoints \mathbf{w}_i ($i = 1, 2, 3$) defined in (16). We
 309 consider two cases: i) There are no obstacles between the waypoints, and ii) There
 310 are two circular obstacles of radii $r_{o_1} = r_{o_2} = 1$ (m) and centers $\mathbf{c}_{o_1} = [-4, 7]^T$ (m)
 311 and $\mathbf{c}_{o_2} = [4, 4]^T$ (m). In the first case, the computed path only has to satisfy the
 312 constraints imposed by the dynamics of the PV. In the second one, the computed
 313 path not only has to satisfy the PV constraints but it also has to avoid colliding
 with the two predefined obstacles. The results are shown in Fig. 6. As can be seen,

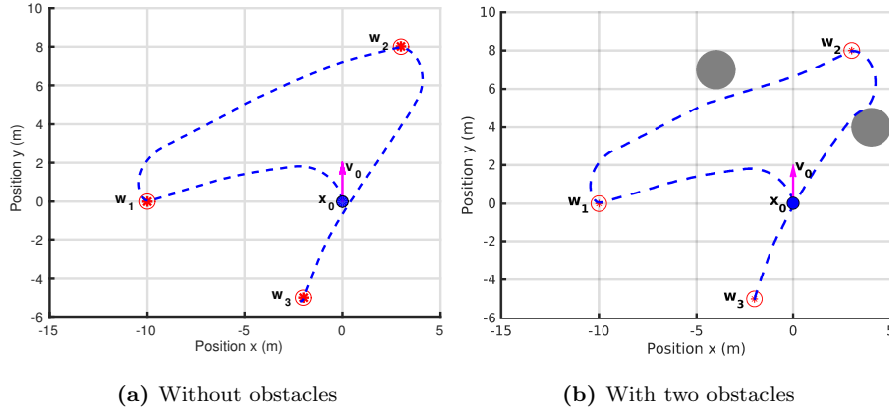


Fig. 6 Computed paths using the path-planning algorithm

314

315 in both cases the PV starts from \mathbf{x}_0 with a velocity vector \mathbf{v}_0 . When there are
 316 no obstacles (Fig. 6a), the resulting path is smooth and it satisfies the PV state
 317 and input constraints. Moreover, the PV passes successfully through the three
 318 desired waypoints. When the two circular obstacles are present (Fig. 6b) the path
 319 is similar to that obtained in the previous case but in this situation the computed

320 path avoids collision with both obstacles. With the proposed methodology, adding
 321 the obstacles is just as simple as adding constraints of the form

$$322 \quad (x - c_{o_{i_x}})^2 + (y - c_{o_{i_y}})^2 \geq r_o \quad (18)$$

323 to the optimization problem (13), where $c_{o_{i_x}}$ and $c_{o_{i_y}}$ denote the x and y compo-
 324 nents of the vector \mathbf{c}_{o_i} . Since the obstacles are added as constraints to (13), their
 325 detection and avoidance is straightforward, because the solution of the optimiza-
 326 tion problem already takes into account the presence of these static obstacles.

327 *Remark 4* Note that any obstacle can be circumscribed within a circle (2D) or a
 328 sphere (3D), thus any shape of obstacle can be considered.

329 Fig. 7 shows the evolution of the velocity modulus and the yaw angle of the
 330 PV for both situations, without obstacles (Fig. 7a) and with them (Fig. 7b).
 331 Both figures are similar, the major difference that they exhibit can be observed
 332 approximately between $t = 21$ (s) and $t = 23$ (s). At this time the PV has reached
 333 the waypoint \mathbf{w}_2 and it is moving towards \mathbf{w}_3 . When the PV detects the presence
 334 of the obstacle centered at \mathbf{c}_{o_2} it must reduce its velocity and modify its yaw angle
 335 in order to avoid colliding with the obstacle. Once the obstacle is avoided, the PV
 336 accelerates again and reaches the final target \mathbf{w}_3 .

337 4.2 Example 2

338 For the second simulation example, we consider that the PV should pass sufficiently
 339 close to waypoints \mathbf{w}_i ($i = 1, 2, 3$) and that there are three obstacles: the previous
 340 two mentioned in example 1, and a third one that appears suddenly at $t = 2.5$ (s).
 341 The latter obstacle is also circular and it is located at $\mathbf{c}_{o_3} = [-6, 2]^T$ (m) with

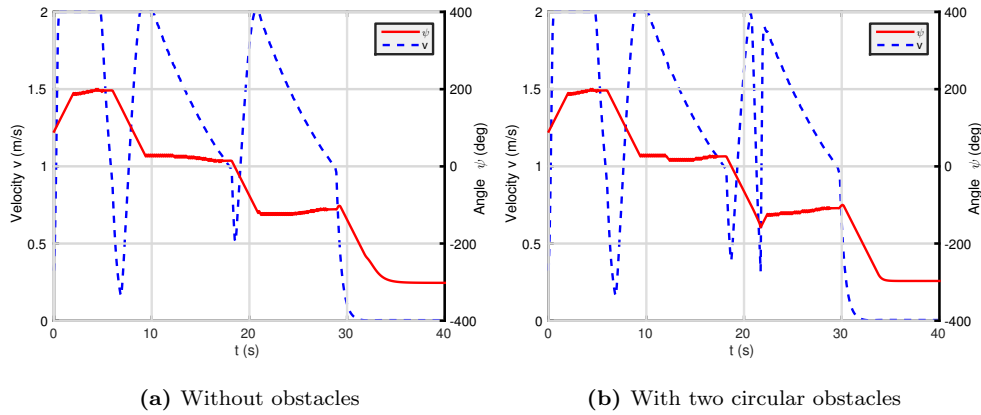


Fig. 7 Evolution of velocity modulus and orientation angle

342 radius $r_{o_3} = 1.5$ (m). The results are shown in Fig. 8. As observed in Fig. 8a,
 343 when the PV starts moving only two fixed obstacles are present. At $t = 2.5$ (s)
 344 (see Fig. 8b) a new circular obstacle appears in the way of the PV. If the PV does
 345 not change the direction of its velocity vector \mathbf{v} , then it will collide with this new
 346 obstacle. Fortunately, we are computing the path in an online manner, so, as it
 347 is shown in Fig. 8c, the PV can detect the new obstacle and the direction of the
 348 velocity vector is automatically changed. In Fig. 8d the resulting path is depicted,
 349 which is smooth and it satisfies not only the PV constraints but also avoids the
 350 two static obstacles and the appearing one. The evolution of the velocity modulus
 351 and the yaw angle is depicted in Fig. 9. As can be observed, a peak appears in the
 352 yaw angle curve between $t = 2.5$ (s) and $t = 4.5$ (s). This occurs because the PV
 353 needs to modify its yaw angle from $\psi = 180$ (deg) up to $\psi = 220$ (deg) in order to
 354 change its direction and, consequently, avoid colliding with the new obstacle. The
 355 evolution of the velocity modulus is similar to that presented in Fig. 7b.

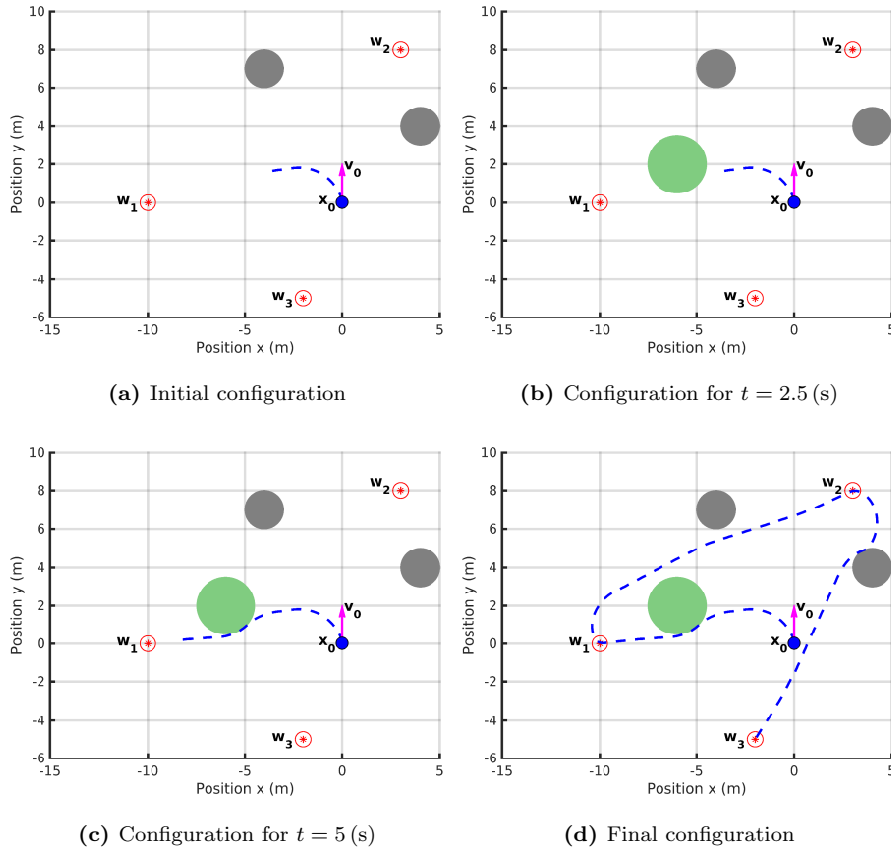


Fig. 8 Generation of a feasible path with two fixed obstacles and one appearing at $t = 2.5$ (s)

356 4.3 Example 3

357 In this example we explore the problem of computing a feasible path in a follower
 358 condition without obstacles. We assume that we have two particle vehicles: PV_1 ,
 359 with initial condition $\mathbf{x}_{0_1} = [0, 0, 0]^T$ and $\mathbf{u}_{0_1} = [\pi/2, 0]^T$, and PV_2 (the follower)
 360 whose initial condition is $\mathbf{x}_{0_2} = [-5, 5, 0]^T$ and $\mathbf{u}_{0_2} = [-\pi/2, 0]^T$. To perform this
 361 simulation example, we configured two NMPC controllers: one for PV_1 and the

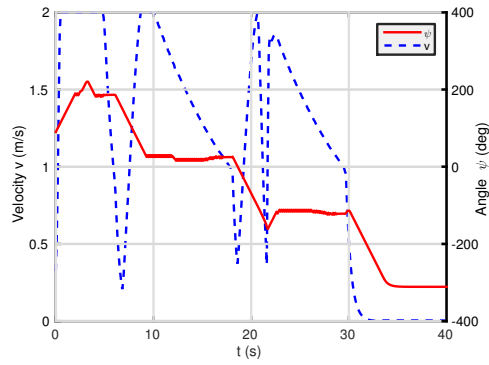


Fig. 9 Evolution of velocity modulus and orientation angle

362 other for PV_2 . The configuration of the NMPC parameters for both controllers
 363 was done as described in the beginning of Section 4, except that we have let PV_2
 364 to increment its speed up to 4 (m/s).

365 In this example, we consider that PV_1 has to reach the waypoint (17) and
 366 PV_2 has to reach PV_1 , i.e. its target is the current position of PV_1 . The results
 367 obtained are shown in Fig. 10. As can be seen in Fig. 10a, at $t = 1.5$ (s) the PV_1
 368 (rounded) starts moving towards w_1 while the PV_2 (squared) modifies its velocity
 369 vector in order to move towards PV_1 . At $t = 3$ (s) (Fig. 10b), the PV_2 is located
 370 behind the PV_1 . When $t = 4.5$ (s) the PV_2 has almost reached the PV_1 and they
 371 both move towards w_1 , as depicted in Fig. 10c. Finally, as shown in Fig. 10d, when
 372 $t = 10$ (s) the PV_2 reaches PV_1 and they both reach the desired target w_1 . Figure
 373 11 compares the velocities (Fig. 11a) and the yaw angles (Fig. 11b) of both PV_1
 374 and PV_2 . As it can be seen from Fig. 11a, the PV_2 increments its speed up to its
 375 maximum value (4 m/s) in order to follow as quick as possible the PV_1 . Once the
 376 follower is close to PV_1 , both velocities profiles are similar. In Fig. 11b it can be
 377 seen how both yaw angles are modified. At $t = 3$ (s) both ψ_1 and ψ_2 have similar

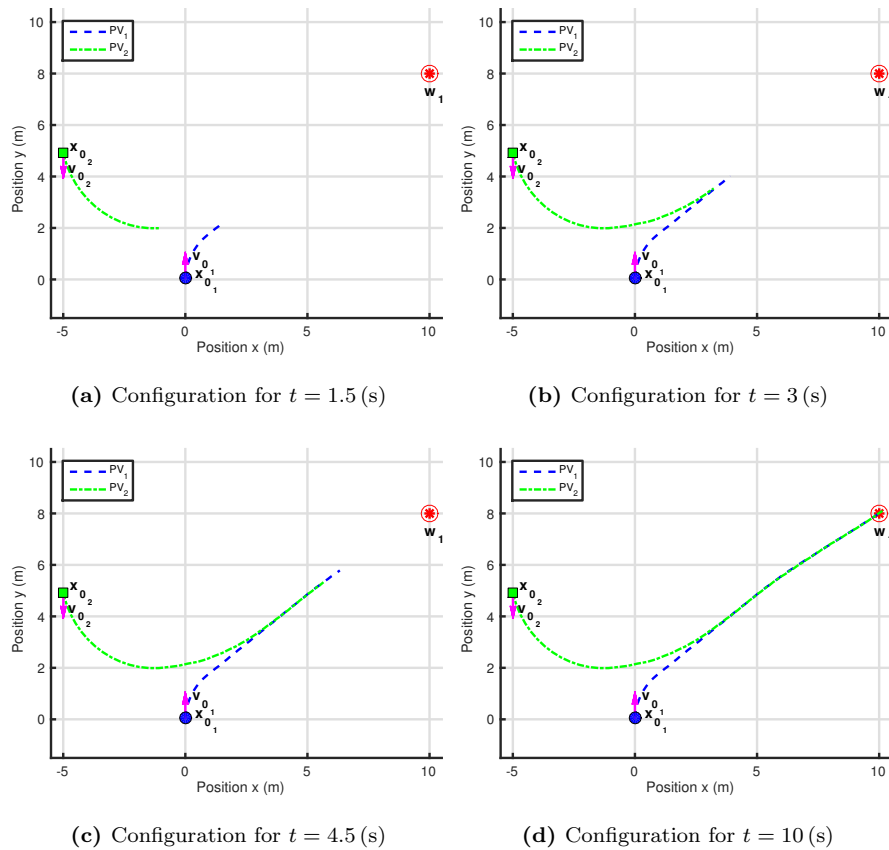


Fig. 10 Generation of a feasible path in a follower condition without obstacles

378 values, meaning that the velocity vectors of PV_1 and PV_2 are aligned with each
 379 other and consequently, PV_1 reaches the desired waypoint and the PV_2 reaches
 380 PV_1 .

381 In this example we have computed a feasible path in a follower problem. If
 382 instead of following the moving object we configure PV_2 to move away from PV_1 ,
 383 then the proposed approach can be easily extended to be used with moving ob-
 384 stacles.

385

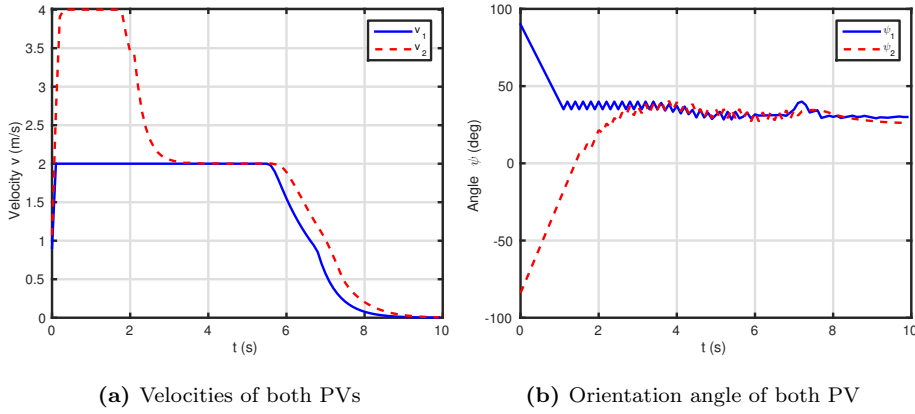


Fig. 11 Evolution of the velocity modulus and orientation angles of both PVs without obstacles

386 4.4 Example 4

387 In this example we explore the problem of computing a feasible path while
 388 following it with a Husky⁹ UGV simulated in Gazebo¹⁰ simulator. The math-
 389 ematical model used to solve the guidance of the Husky UGV is given by the
 390 following equation

$$391 \quad \dot{\mathbf{x}} = f(\mathbf{x}, \mathbf{u}) = \begin{bmatrix} v_h \cos \psi_h \\ v_h \sin \psi_h \\ \omega_h \end{bmatrix}, \quad (19)$$

392 where $\mathbf{x} = [x_h, y_h, \psi_h]^T$ is the state vector, x_h and y_h denote the robot position
 393 and ψ_h denotes its yaw angle. The control input vector $\mathbf{u} = [v_h, \omega_h]^T$ includes the
 394 linear and angular velocities v_h and ω_h , respectively. It should be noticed that
 395 the model (19) used to control the Husky is different from the plant, which is

⁹ <https://www.clearpathrobotics.com/husky-unmanned-ground-vehicle-robot/>

¹⁰ <http://gazebosim.org/>

396 a complex model simulated by Gazebo. We assume that both the PV and the
 397 Husky UGV have the same initial position but they differ in its initial orientation
 398 angle. The PV has its velocity vector pointing upwards ($\psi = 90(\text{deg})$) while the
 399 Husky velocity vector points to the east side ($\psi_h = 0(\text{deg})$). As it can be seen in
 400 Fig. 12 the Husky model is able to follow the computed path successfully. This is
 401 mainly due to the fact that the navigation algorithm generates a trajectory that
 is feasible and takes into account the dynamic constraints of the UGV. Fig. 13a

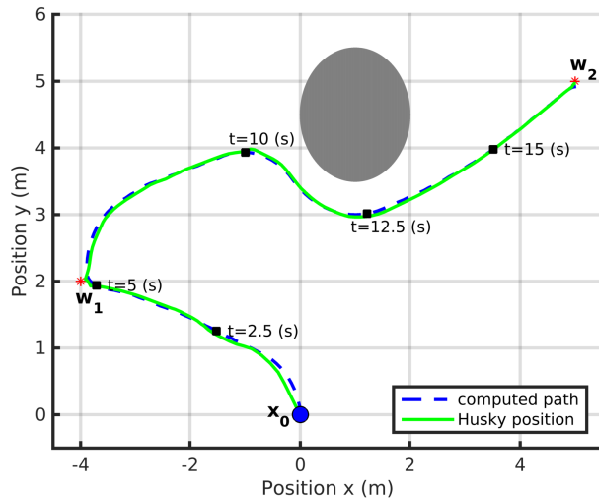


Fig. 12 Path-following with a Husky UGV

402
 403 shows that when $t = 0(s)$, the Husky turns left in order to move towards waypoint
 404 $\mathbf{w}_1 = [-4, 2, 0.5]^T$. Once it is reached, the Husky UGV turns right in order to move
 405 in a straight line towards waypoint $\mathbf{w}_2 = [5, 5, 0]^T$. As the path was computed
 406 taking into account a circular obstacle which is located at $\mathbf{c}_o = [1, 4.5]^T$ (m) with
 407 radius $r_o = 1$ (m), it can be seen that the UGV performs the obstacle avoidance
 408 maneuver at approximately $t = 10(s)$ without any difficulty. After that, it moves

409 towards waypoint w_2 in almost a straight line. It should be emphasized that as
 410 the resulting path is smooth and feasible, the Husky is able to follow it without
 411 major difficulties. In Fig. 13b it is shown the xy -position errors $e_x = x - x_h$ and
 412 $e_y = y - y_h$, respectively, in the path-following maneuver. It can be seen that at
 413 approximately $t = 1$ (s) both errors tend to increase. This is due to the fact that
 414 the orientation of the Husky is different from the orientation of the PV. This was
 415 done on purpose in order to show that despite both yaw angles were different, the
 416 Husky is able to follow quite well the computed path. Then, for approximately
 $t > 2.5$ (s) the position errors tend to decrease and are very close to 0.

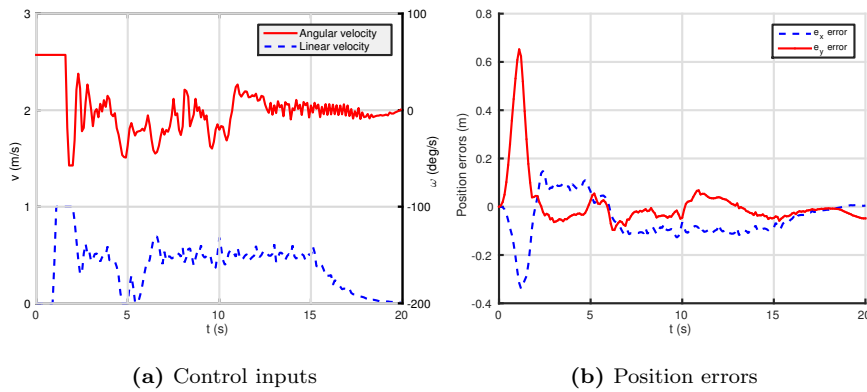


Fig. 13 Husky control inputs and path-following errors

417

418 5 Conclusions

419 In this article we have presented an online path-planning algorithm that can be
 420 used to guide any kind of unmanned vehicle towards desired targets. The pro-
 421 posed algorithm handles the problem of finding the optimal path towards desired

422 waypoints, while taking into account the kinematic, the dynamic and constraint of
423 the vehicle. We used a simplified particle vehicle model and the iterated non-linear
424 model predictive control technique to control the velocity vector of this particle
425 vehicle model. By controlling this vector we have actually determined the path
426 that the particle vehicle model should take in order to reach the targets. We have
427 also exploited the use of a higher order cost function in the optimization problem.
428 Because we have used the iterated NMPC algorithm [16], optimality, stability and
429 feasibility can be guaranteed. The performance and capabilities of the proposed
430 path-planning algorithm were demonstrated through several simulation examples.
431 [The path-following capabilities were explored using a Husky UGV to follow a](#)
432 [feasible path. All the simulation examples were performed successfully.](#)

433 **Acknowledgements** The authors wish to thank the *Universidad Nacional de Litoral* (with
434 CAI+D Jóven 500 201501 00050 LI and CAI+D 504 201501 00098 LI), the *Agencia Nacional*
435 *de Promoción Científica y Tecnológica* (with PICT 2016-0651) and the *Consejo Nacional de*
436 *Investigaciones Científicas y Técnicas* (CONICET) from Argentina, for their support.

437 **References**

- 438 1. P. Doherty and P. Rudol, “A uav search and rescue scenario with human body
439 detection and geolocalization,” *Lecture Notes in Computer Science*, pp. 1–13,
440 2007.
- 441 2. G. E. Dewi Jones & Ian Golightly, Jonathan Roberts & Kane Usher, “Power
442 line inspection-a UAV concept,” in *IEE Forum on Autonomous Systems*,
443 no. November, pp. 2–7, 2005.

- 444 3. C. Zhang and J. Kovacs, “The application of small unmanned aerial systems
445 for precision agriculture: a review,” 2012.
- 446 4. S. M. Adams, M. L. Levitan, and C. J. Friedland, *High Resolution Imagery*
447 *Collection Utilizing Unmanned Aerial Vehicles (UAVs) for Post-Disaster Studies*,
448 ch. 67, pp. 777–793. American Society of Civil Engineers, 2013.
- 449 5. A. Bouhraoua, N. Merah, M. AlDajani, and M. ElShafei, “Design and imple-
450 mentation of an unmanned ground vehicle for security applications,” in *7th*
451 *International Symposium on Mechatronics and its Applications (ISMA)*, pp. 1–6,
452 April 2010.
- 453 6. M. YAĞIMLI and H. S. Varol, “Mine detecting gps-based unmanned ground
454 vehicle,” in *4th International Conference on Recent Advances in Space Technolo-*
455 *gies*, pp. 303–306, 2009.
- 456 7. United States Air Force, “Unmanned aircraft systems flight plan 2009–2047,”
457 *Headquarters Department of the Air Force, Washington DC*, 2009.
- 458 8. Weatherington, Dyke and Deputy, U, “Unmanned aircraft systems roadmap,
459 2005–2030,” *UAV Planning Task Force, OUSD (AT&L)*, 2005.
- 460 9. S. M. LaValle, *Planning algorithms*. Cambridge university press, 2006.
- 461 10. M. Saska, V. Spurn, and V. Vonek, “Predictive control and stabilization of
462 nonholonomic formations with integrated spline-path planning,” *Robotics and*
463 *Autonomous Systems*, 2015.
- 464 11. Q. Xue, P. Cheng, and N. Cheng, “Offline path planning and online replanning
465 of uavs in complex terrain,” in *Proceedings of 2014 IEEE Chinese Guidance,*
466 *Navigation and Control Conference*, pp. 2287–2292, 2014.
- 467 12. G. Zhang and X. Zhang, “A novel DVS guidance principle and robust adap-
468 tive path-following control for underactuated ships using low frequency gain-

-
- 469 learning,” *ISA Transactions*, vol. 56, pp. 75 – 85, 2015.
- 470 13. Yang, Liang and Qi, Juntong and Song, Dalei and Xiao, Jizhong and Han,
471 Jianda and Xia, Yong, “Survey of Robot 3D Path Planning Algorithms,” *Jour-*
472 *nal of Control Science and Engineering*, vol. 2016, 2016.
- 473 14. M. Hehn and R. D’Andrea, “Real-time trajectory generation for quadro-
474 copters,” *IEEE Transactions on Robotics*, vol. 31, no. 4, pp. 877–892, 2015.
- 475 15. Minh, Vu Trieu and Pumwa, John, “Feasible path planning for autonomous
476 vehicles,” *Mathematical Problems in Engineering*, vol. 2014, 2014.
- 477 16. M. Murillo, G. Snchez, and L. Giovanini, “Iterated non-linear model predictive
478 control based on tubes and contractive constraints,” *ISA Transactions*, vol. 62,
479 pp. 120 – 128, 2016.
- 480 17. F. Gavilan, R. Vazquez, and E. F. Camacho, “An iterative model predictive
481 control algorithm for uav guidance,” *IEEE Transactions on Aerospace and Elec-*
482 *tronic Systems*, vol. 51, no. 3, pp. 2406–2419, 2015.
- 483 18. G. Sanchez, A. Limache, L. Giovanini, and M. Murillo, “Distributed model pre-
484 dictive control based on dynamic games,” in *Advanced Model Predictive Control*
485 (T. Zheng, ed.), ch. 4, pp. 65–90, InTech, 7 2011.
- 486 19. Joel Andersson, *A General-Purpose Software Framework for Dynamic Optimiza-*
487 *tion*. PhD thesis, Arenberg Doctoral School, KU Leuven, Department of
488 Electrical Engineering (ESAT/SCD) and Optimization in Engineering Cen-
489 ter, Kasteelpark Arenberg 10, 3001-Heverlee, Belgium, October 2013.

490 **M. Murillo** received the Ph.D degree in Engineering Science, computational intel-
491 ligence, signals and systems mention from Universidad Nacional del Litoral (Ar-
492 gentina) in 2015. She is currently a post-doctoral student in the *Instituto de In-*
493 *vestigación en Señales, Sistemas e Inteligencia Computacional* (Research Institute for
494 Signals, Systems and Computational Intelligence) at the Facultad de Ingeniería
495 y Ciencias Hídricas, Universidad Nacional del Litoral (Argentina). Her research
496 interests include nonlinear control theory and its applications to aerial vehicles
497 simulation, navigation and control.

498 **Guido Sánchez** received the Ph.D degree in Engineering Science, computational
499 intelligence, signals and systems mention from Universidad Nacional del Litoral
500 (Argentina) in 2017. He is currently a post-doctoral student in the *Instituto de In-*
501 *vestigación en Señales, Sistemas e Inteligencia Computacional* (Research Institute for
502 Signals, Systems and Computational Intelligence) at the Facultad de Ingeniería
503 y Ciencias Hídricas, Universidad Nacional del Litoral (Argentina). His research
504 interests include estimation and control of dynamical systems, multi-agent coop-
505 erative control and navigation and control of mobile robots.

506 **Lucas Genzelis** received the BSc degree in Informatics Engineering from Univer-
507 sidad Nacional del Litoral (Argentina) in 2015. He is currently a Ph.D. student
508 at the *Instituto de Investigación en Señales, Sistemas e Inteligencia Computacional*
509 (Research Institute for Signals, Systems and Computational Intelligence) at the
510 Facultad de Ingeniería y Ciencias Hídricas, Universidad Nacional del Litoral (Ar-

511 gentina). His research interests are mainly focused on autonomous navigation of
512 flying vehicles and on identification of dynamical systems.

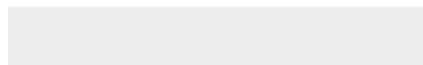
513 **Leonardo Giovanini** received the Ph.D. degree in Engineering Science from Uni-
514 versidad Nacional del Litoral (Argentina) in 2000. He was Senior Research Fellow
515 and Technical Manager of the Industrial Control Center, University of Strathclyde
516 (United Kingdom), from 2001 until 2007. In 2008 he joined to the *Instituto de In-*
517 *vestigación en Señales, Sistemas e Inteligencia Computacional* (Research Institute for
518 Signals, Systems and Computational Intelligence), at the Universidad Nacional del
519 Litoral, and the National Council of Technological and Scientific Research (CON-
520 ICET). His research interests are mainly related to robust and nonlinear control
521 theory including robust adaptive control, model predictive control and modelling
522 and analysis of multi-agent systems. Application fields are robotics, autonomous
523 vehicles and multi-agent systems.

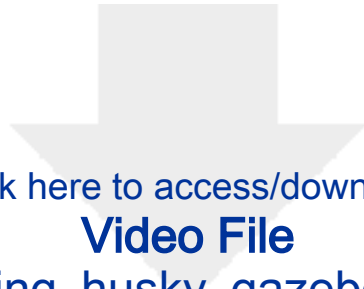


[Click here to access/download](#)

Video File

[path_planning_husky_gazebo_video.m4v](#)





Click here to access/download

Video File

path_planning_husky_gazebo_video.ogv

